Flexible Phototransistors Based on Single-Crystalline Silicon Nanomembranes

*Jung-Hun Seo, Kan Zhang, Munho Kim, Deyin Zhao, Hongjun Yang, Weidong Zhou, and Zhenqiang Ma**

In this work, flexible phototransistors with a back gate configuration based on transferrable single-crystalline Si nanomembrane (Si NM) have been demonstrated. Having the Si NM as the top layer enables full exposure of the active region to an incident light and thus allows for effective light sensing. Flexible phototransistors are performed in two operation modes: 1) the high light detection mode that exhibits a photo-to-dark current ratio of 10^5 at voltage bias of $V_{GS} < 0.5$ V, and $V_{DS} = 50$ mV and 2) the high responsivity mode that shows a maximum responsivity of 52 A W^{-1} under blue illumination at voltage bias of $V_{GS} = 1$ V, and $V_{DS} = 3$ V. Due to the good mechanical flexibility of Si NMs with the assistance of a polymer layer to enhance light absorption, the device exhibits stable responsivity with less than 5% of variation under bending at small radii of curvatures (up to 15 mm). Overall, such flexible phototransistors with the capabilities of high sensitivity light detection and stable performance under the bending conditions offer great promises for high-performance flexible optical sensor applications, with easy integration for multifunctional applications.

1. Introduction

Photodetectors are one of the indispensable components for most optoelectronic applications due to their ability to convert light signals into electrical signals.[1] Compared with the renowned III–V compound photodetectors, silicon (Si) photodetectors can be easily integrated with the conventional Si-based complementary metal oxide semiconductor (CMOS) technology, and this compatibility explains why silicon photonics is attracting growing research interest in recent years.[2] Although conventional p–n and p–i–n photodiodes are the most popular device structures, they suffer from low responsivity and quantum efficiency.[3] Therefore, it is necessary to boost an electrical signal to an acceptable range via amplifiers.[4] In recent years, research has revealed that the metal oxide semiconductor field-effect transistors (MOSFETs) exhibit exceptional photosensing capability.[5,6,24] MOSFET-type photodetectors, also known as phototransistors, have the advantages of not only high photosensitivity and responsivity, but also integrability into conventional CMOS chips. However, some shortcomings still exist due to structural limitations such as limited light-sensing area and light blocking by gate electrodes. More importantly, these devices have been built on a rigid substrate, making it difficult to manipulate the physical shape of the photodetector. Mechanical flexibility can bring another important degree of freedom in designing phototransistors, while maintaining high performance.[7,8] With recent advances in transferrable single-crystalline silicon nanomembranes (Si NM),[8,9] it is possible to demonstrate various flexible electronic and optoelectronic devices such as p–i–n photodiodes,[10,11] thin-film transistors,[12–17] microwave switches,[18,19] and solar cells.[20] These devices exhibit excellent electrical and optical characteristics under bending and stretching conditions.

In this paper, we report the demonstration and comprehensive performance characterizations of thin-film transistor-type flexible phototransistors using single-crystalline Si NMs. The phototransistors were designed to maximize light sensing by the flip transfer of their Si NM layer, and the gate stack and source/drain electrodes (called silicon-on-top structure). In this structure, unlike other MOSFET-type photodetectors, light absorption in a Si NM layer can be much more efficient because light is not blocked by any metal layers or other materials. Also, the active region, where light is detected, is not limited by channel dimension. Moreover, electrodes placed underneath the Si NM also acted as light reflectors to further improve light absorption. Therefore, these two design merits led to very high responsivity, despite the use of thin Si NMs (i.e., only 270 nm). Overall, flexible Si NM phototransistors exhibit not only a sufficient light/dark current ratio when working at a very low voltage bias, but also very high responsivity when working at a normal operation voltage bias.

2. Results and Discussion

The schematic illustration of the device fabrication is shown in **Figure 1**. The fabrication detail can be found in Experimental Section, but in short, the process began with n+ doping in SOI

Dr. J.-H. Seo, Dr. K. Zhang, M. Kim, Prof. Z. Ma
Department of Electrical and Computer Engineering
University of Wisconsin-Madison
Madison, WI 53706, USA
E-mail: mazq@engr.wisc.edu
Dr. D. Zhao, Dr. H. Yang, Prof. W. Zhou
Department of Electrical Engineering
University of Texas at Arlington
Arlington, TX 76019, USA

DOI: 10.1002/adom.201500402

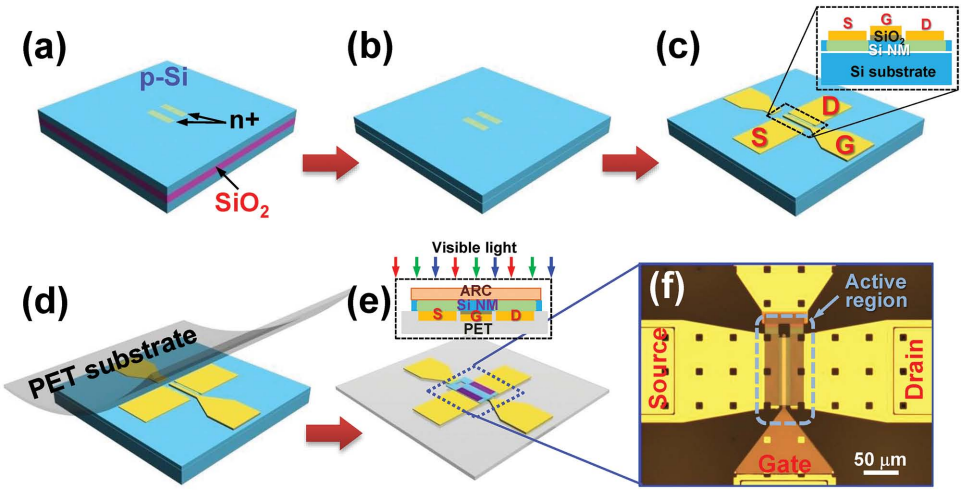

Figure 1. The schematic illustration of the device fabrication process flow; a) Beginning with forming n^+ regions by ion implantation of source/drain regions to achieve an ohmic contact, b) Releasing Si NM by selective etching of a buried oxide layer; c) Metallization by e-beam evaporation to deposit source/drain electrodes, and a stack of gate/gate dielectric, d) Transfer printing fully fabricated devices to adhesive layer-coated PET substrate, e) Spin-coating a protection layer on top of the surface, f) Microscopic image of a finished flexible phototransistor. Insets in (c) and (e) depict the cross-sectional view of device.

wafer (SOITEC) (Figure 1a), followed by separation of the top Si layer (Si NM) (Figure 1b). Gate and source/drain electrodes were deposited by e-beam evaporation (Figure 1c). After the metallization step, the entire device layers (metal electrodes and Si NM) were flip transferred to an adhesive layer (SU-8 2002, Microchem) coated with polyethylene terephthalate (PET) substrate and cured (Figure 1d). The active layer was defined (Figure 1e) and covered by an anti-reflection coating (ARC) layer (SU-8 2002). The ARC layer has a refractive index (n) between 1.57 and 1.65 for visible light[25] with the average optical transmittance in the visible range of nearly 97%.[28] Thus, it reduces light reflection and enhances light transmission into the Si NM and consequently improves light absorption by the Si NM. Detailed descriptions on the transfer printing process and ion implantation can be found elsewhere.[21] Shown in Figure 1f is a micrograph of the fabricated phototransistor. It can be clearly seen that the Si NM where light is sensed lies on the top of the gate stack and source/drain electrodes. Therefore, the incident light is not blocked by any of the layers.

The light sensing characteristics were measured under dark and illuminated conditions by using representative Si NM phototransistors, which have a channel width and channel length of 50 μm and 2 μm, respectively. As shown in **Figure 2**, the phototransistor can be operated in two different modes: the first mode is for the high photo-to-dark current ratio by operating under low voltage biases, and the second mode is for the high responsivity under high voltage biases. In the first mode, phototransistors showed extremely low dark current (<10 pA) and high photocurrent (i.e., drain current) (>0.4 μA) under very low voltage bias (V_{GS} < 0.5 V, and V_{DS} = 50 mV), which yields a photo-to-dark current ratio of up to 10^5 times. As gate bias is increased, the transistor current substantially increases due to the transistor effect and the photo-to-dark current ratio thus decreases to 11 times. This indicates that the devices are suitable for operation in the first mode under very low bias. The observed dark current is comparable with that of conventional p–i–n photodiodes and other NMOSFET photodetectors.[22,23] The very high photo-to-dark current ratio is attributed to the silicon-on-top structure, better light absorption with the SU-8 ARC layer, and with metal electrodes as reflectors.

To prove the effectiveness of light absorption enhancement of the ARC and the metal reflector, optical simulations were performed. Figure 2b shows the simulated light absorptions of Si NM in the visible wavelength range (400–700 nm) before adding any light absorption-assisted layers (Case 1), after applying the metal electrode as a reflector (Case 2), and applying both the SU-8 ARC layer and the metal reflector (Case 3). It should be noted that the simulations were performed based on the actual layer thicknesses and optical parameters. The averaged light absorption of Si NM in the visible wavelength region nearly doubled from 20.2% to 38.3% with the metal reflector on the backside of the Si NM. In addition, the SU-8 ARC layer on the top of the Si NM further enhances its average light absorption from 38.3% to 48%, which is equivalent to using a 480 nm thick Si NM. Particularly, light absorption of the Si NM in blue, green, and red wavelengths increases from 44%, 20%, and 5% to 99%, 99%, and 40%, respectively, by adding the metal reflector and the ARC layer.

In Figure 2c, I_{DS}–V_{DS} characteristics under red, green, and blue laser sources are shown. When the phototransistors are biased at higher voltages, they operate in the second mode where high responsivity is achieved. Responsivity "R" in phototransistors can be calculated Equation[23] (1) $R = I_{ph}/P_{inc} = I_{ph}/(E \times A)$, where I_{ph} is the photocurrent, P_{inc} is the light power incident onto the active region of the device, E is the irradiance of the incident light (power intensity), and A is the area of the active region. According to Equation (1), when the incident light was reflected back to the active region by the bottom metal reflector and the top ARC layer, the light absorption to the active region nearly doubled, which is equivalent to half of the P value. Therefore, the enhanced light absorption in the active region is the major factor in the improved responsivity of the devices. In this

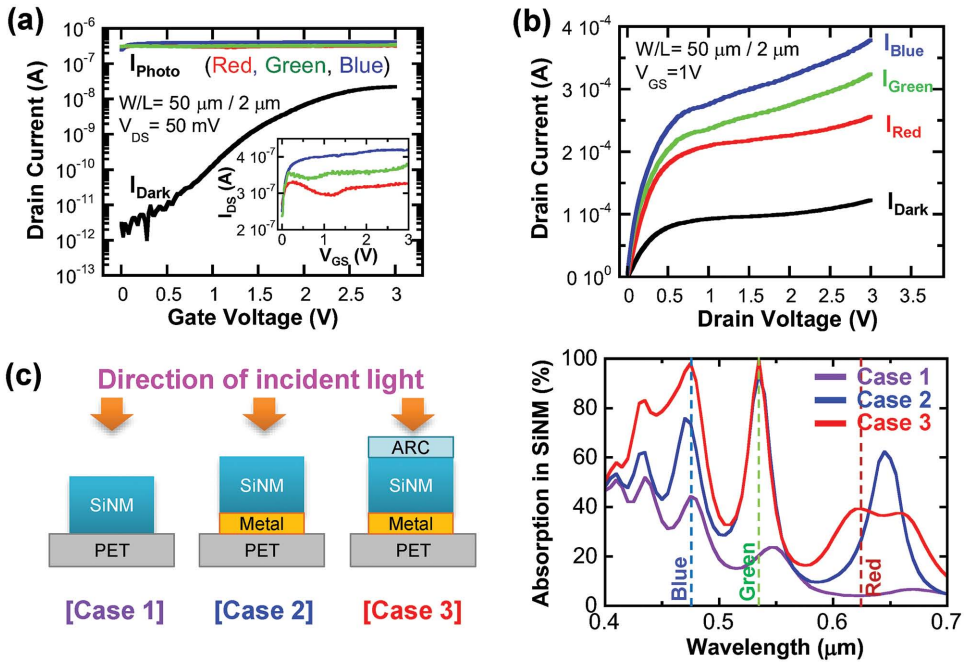

Figure 2. a) Drain current–gate voltage characteristics (I_{DS}–V_{GS}) at V_{DS} = 0 V. Inset shows the magnified plot of photo currents. b) Drain current–drain voltage characteristics (I_{DS}–V_{GS}) under dark and illumination with various light sources (red, green, and blue) onto flexible phototransistors. I_{DS}–V_{GS} curve under V_{GS} = 1 V for photo-to-dark current ratio shows as high as ≈1×10^5. c) (left) Three layer structures used to simulate the light absorption of Si NM, (right) and their corresponding simulated absorption of Si NM i) without any layers, ii) with the metal reflector underneath the Si NM, iii) with the metal reflector underneath the Si NM and SU-8 ARC layer on the top of Si NM, respectively. Dashed line denotes blue (473 nm), green (532 nm), and red (632 nm) wavelengths.

calculation, ≈4 mW mm^{-2} of E and 2000 μm^2 of A are used. It should be noted that the area of the active region refers to the size of the entire Si NM, including the channel region and contact region, due to the Si NM-on-top structure. The responsivity at voltage bias of V_{GS} = 1 V and V_{DS} = 3 V under red, green, and blue light illumination are calculated to be 51, 41, and 18 A W^{-1}, respectively. It should be noted that the responsivity under low gate bias, which is the first mode, only shows 0.04 A W^{-1}. Considering the responsivity value of ≈1 A W^{-1} from the amorphous Si phototransistor deposited on a glass substrate, which has a similar layer thickness to our Si NM phototransistor,[29] these responsivity values are relatively high considering the thin Si NM used in the device. We believe that the increasing spectral responsivities at decreasing wavelength of light could be attributed to the increase in absorption coefficients of Si in the visible light range.[26] To investigate the effect on photocurrent with various dimensions in the Si NM-active regions, phototransistors with different channel areas (W/L = 25/2, 50/2, 50/10, 100/10 μm) were measured under dark and green light illumination conditions (532 nm) as shown in **Figure 3**. As expected from the equation[27]: (2) $I_D = 0.5 \cdot \mu \cdot C_{ox} \cdot (W/L) \cdot (V_{GS} - V_t)^2$, where W and L are the channel width and length, the device with a larger W/L ratio shows higher photocurrent. It was also observed that the device with a larger L value shows better light sensitivity if the W/L ratio is fixed. As shown in Figure 3a,d, which have similar W/L ratios, the device with L = 10 μm showed 2.35 times of the photo-to-dark current increment at V_{GS} = 1 V and V_{DS} = 3 V, while the device with L = 2 μm only showed 1.3 times of increment.

The responsivities under red, green, and blue light illuminations as a function of channel length are shown in **Figure 4**a. Responsivities decrease with the increase in channel length from 2 to 10 μm. The trend agrees well with the relationship between the channel current and the responsivity given to Equation (3): $R = 0.5 \cdot \mu \cdot C_{ox} \cdot (V_{GS} - V_{th})^2 / (L^2 \cdot P)$ by incorporating Equation (1) and Equation (2). Therefore, the device with a smaller channel length is more suitable for the second operation mode, which is for high responsivity. Figure 4b shows the responsivity measured using red (632 nm), green (532 nm), and blue (473 nm) laser sources under the bending condition of external uniaxial strain of 1.08% and 0.2% for tensile and compressive strain, respectively (measured from bending curvature). An optical image of the flexible Si NM phototransistor on a bent substrate is shown in Figure 4c. The responsivities were measured from the device whose W/L is 50/2 μm under green light. It is speculated that the increase in the responsivity is attributed to the mobility enhancement in the crystal structure of Si NM, which is commonly observed in Si NM-based flexible devices.[15,16] The bendable characteristics of the phototransistors make them suitable for a number of important applications, such as wide view angle imaging.[30,31]

The drain current as a function of time is shown in Figure 4d. The 1 millisecond (msec) purse mode green laser was used as a light source and the waveform was recorded by the digital oscilloscope (Tektronics TDS1000C). We used the same device and light sources for the bending experiment. The device showed 0.05 msec and 0.11 msec of the rise and fall

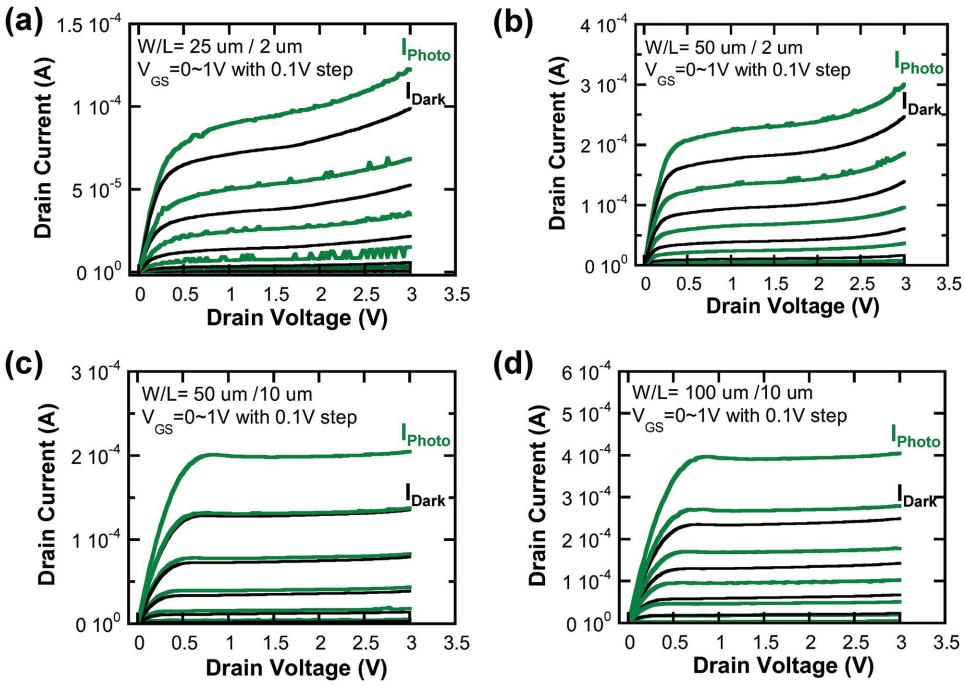

Figure 3. Drain current–drain voltage characteristics (I_{DS}–V_{DS}) with different V_{GS} biases ranging from 0 to 1 V with a 0.1 V step under the dark and the green light illumination to flexible phototransistors, which have different W/L ratios: a) $W = 25$ μm, $L = 2$ μm, b) $W = 50$ μm, $L = 2$ μm, c) $W = 50$ μm, $L = 10$ μm, d) $W = 100$ μm, $L = 10$ μm.

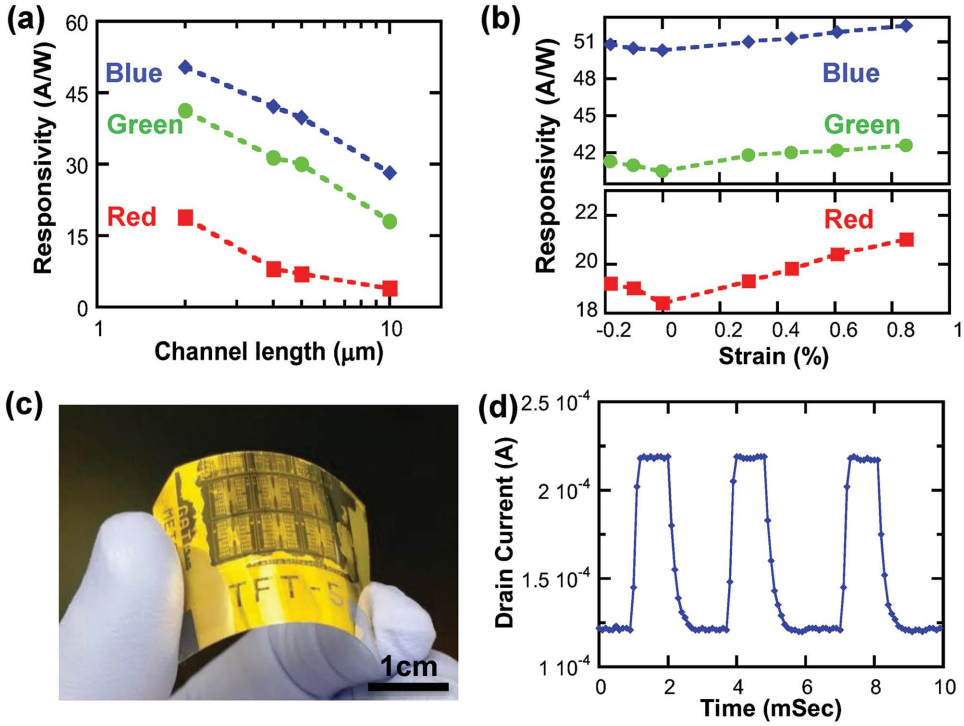

Figure 4. a) A trend of responsivity with respect to channel lengths from 2 to 10 μm. The channel width and bias point were fixed at 50 μm and at $V_{GS} = 1$ V and $V_{DS} = 3$ V. b) Responsivity under bending condition measured at a fixed voltage bias point of $V_{GS} = 1$ V and $V_{DS} = 3$ V. c) An optical image of the flexible Si NM phototransistor on a bent substrate. d) Modulated photocurrent under pulsed 5 mW green laser measured at a fixed voltage bias of $V_{GS} = 1$ V and $V_{DS} = 3$ V.

times, which are very similar to the previously reported phototransistors on rigid substrates.[5] No overshooting and oscillating were observed.

3. Conclusion

In summary, we have demonstrated flexible Si NM phototransistors on PET substrate. The silicon-on-top structure with the light absorption layer enables achievement of high light sensitivity and responsivity under different operation modes. The phototransistor exhibits a maximum responsivity of 52 A W^{-1} under blue illumination and the photo-to-dark current ratio of more than 10^5 times under green light illumination. The phototransistor also shows very good mechanical flexibility without any performance degradation. Overall, flexible phototransistors with the capabilities of high sensitivity photo detection and stable performance under the bending condition provide great potentials in high performance and flexible photo-detection systems.

4. Experimental Section

Device Fabrication: The fabrication began with an SOI wafer (SOITEC), which has a 270 nm lightly p-type doped (boron, ≈1 × 10^{15} cm^{-3}) top Si layer and a 200 nm buried oxide layer. Two n^+ well regions (≈8 × 10^{19} cm^{-3}) were formed by phosphorous ion implantation, followed by a diffusion process at 850 °C for 40 min in the furnace with nitrogen gas (Figure 1a). After forming releasing holes, the top Si layer, now called Si NM, was released from the buried oxide layer by selective wet-etching in concentrated HF (49%). The released top Si NM gently fell down onto the handling Si substrate (Figure 1b). After rinsing and drying the sample, the Si NM was weakly bonded to the handling Si substrate via Van der Waals forces. Gate stack (SiO_2/Ti/Au 100 nm/20 nm/80 nm) and source/drain electrodes (Ti/Au 20 nm/180 nm) were patterned using e-beam lithography and deposited by e-beam evaporation (Figure 1c). After the completion of the metallization step, the entire device layers (metal electrodes and Si NM) were flip transferred to an 0.6 μm thick adhesive layer (SU-8 2002, Microchem) coated with polyethylene terephthalate (PET) substrate, and cured to glue the devices onto the PET substrate (Figure 1d). After the transfer step, the Si NM layer is positioned face-up and the electrodes were buried underneath the Si NM. The active layer was defined by the photoresist patterning and dry etching steps (Figure 1e). Finally, the entire device was covered by an anti-reflection coating (ARC) layer (SU-8 2002).

Improved Transfer Printing Method: With the conventional transfer printing technique, the semiconductor nanomembrane can be transferred on either a flat or a curvy surface with a yield of nearly 100%.[8,9] However, the position of the transferred semiconductor nanomembrane can be slightly changed during the fabrication process due to the different thermal expansions between the plastic substrate and the adhesion layer.[14] The improved transfer printing technique we used in this work, i.e., releasing a Si nanomembrane and then transfer printing the finished devices, enables to avoid such issues effectively. The critical parameter in order to use this method is to have a thin buried oxide layer so as to increase the Van der Waals force to hold the released Si nanomembrane during the rest of fabrication process. It was discovered that the new method can be used for a box layer with a thickness thinner than 200 nm.

Device Characterization: I–V characteristics of the fabricated devices under dark and illumination were measured using a semiconductor parameter analyzer (HP4155B). The photosensitivity of devices were also characterized using three different laser sources (473 nm (blue), 532 nm (green), and 632 nm (red) wavelengths) with the same power intensity of 4 mW mm^{-2}.

Simulation of Absorption in Si NM: The simulation was carried out by using a 3D finite-difference time-domain (3D FDTD) technique in the visible light region (400 to 700 nm) where the refractive indices of Si NM and SU-8 used in the simulation are 3.48 and 1.57–1.65 for visible light wavelength, respectively. For simplicity and numerical expediency, the study is limited to surface normal incidence. It has been also assumed that the size and thickness of designed pattern are same as the size of the active region.

Acknowledgements

J.-H.S. and K.Z. contributed equally to this work. The work was supported by the Air Force Office of Scientific Research (AFOSR): Presidential Early Career Award in Science & Engineering (PECASE) grant # FA9550-09-1-0482. The program manager is Dr. Gernot Pomrenke.

Received: July 21, 2015
Revised: August 23, 2015
Published online: October 26, 2015

[1] Y. Kang, H.-D. Liu, M. Morse, M. J. Paniccia, M. Zadka, S. Litski, G. Sarid, A. Pauchard, Y.-H. Kuo, H.-W. Chen, W. S. Zaoui, J. E. Bowers, A. Beling, D. C. McIntosh, X. Zheng, J. C. Campbell, *Nat. Photonics* **2009**, *3*, 59.
[2] C. Gunn, *IEEE Compd. Semicond. Integr. Circuit Symp.* **2006**, 139.
[3] J. Michel, L. Jifeng, L. C. Kimerling, *Nat. Photonics* **2010**, *4*, 527.
[4] E. Cabruja, M. Bigas, J. Forest, J. Salvi, *Microelectron. J.* **2006**, *37*, 433.
[5] H. Yamamoto, K. Taniguchi, C. Hamaguchi, *Jpn. J. Appl. Phys.* **1996**, *35*, 1382.
[6] Z. Weiquan, C. Mansun, S. K. H. Fung, P. K. Ko, *IEEE Electron Device Lett.* **1998**, *19*, 435.
[7] H.-C. Yuan, J. Shin, G. Qin, L. Sun, P. Bhattacharya, M. G. Lagally, G. K. Celler, Z. Ma, *Appl. Phys. Lett.* **2009**, *94*, 013102.
[8] J. A. Rogers, T. Someya, Y. Huang, *Science* **2010**, *327*, 5973.
[9] J. A. Rogers, M. G. Lagally, R. G. Nuzzo, *Nature* **2011**, *477*, 45.
[10] Y. Weiquan, Y. Hongjun, Q. Guoxuan, M. Zhenqiang, J. Berggren, M. Hammar, R. Soref, Z. Weidong, *Appl. Phys. Lett.* **2010**, *96*, 121107.
[11] J.-H. Seo, T. Y. Oh, J. Park, W. Zhou, B. K. Ju, Z. Ma, *Adv. Funct. Mater.* **2013**, *2723*, 3398.
[12] H.-C. Yuan, Z. Ma, M. M. Roberts, D. E. Savage, M. G. Lagally, *J. Appl. Phys.* **2006**, *100*, 013708.
[13] H.-C. Yuan, G. K. Celler, Z. Ma, *J. Appl. Phys.* **2007**, *102*, 034501.
[14] L. Sun, G. Qin, J.-H. Seo, G. K. Celler, W. Zhou, Z. Ma, *Small* **2010**, *6*, 2553.
[15] H. Zhou, J.-H. Seo, D. M. Paskiewicz, Y. Zhu, G. K. Celler, P. M. Voyles, W. Zhou, M. G. Lagally, Z. Ma, *Sci. Rep.* **2013**, *3*, 1291.
[16] G. Qin, J.-H. Seo, Y. Zhang, H. Zhou, W. Zhou, Y. Wang, J. Ma, Z. Ma, *IEEE Electron. Device Lett.* **2013**, *34*, 262.
[17] J.-H. Seo, T.-H. Chang, J. Lee, R. Sabo, W. Zhou, Z. Cai, S. Gong, Z. Ma, *Appl. Phys. Lett.* **2015**, *106*, 262101.
[18] G. Qin, H.-C. Yuan, Y. Qin, J.-H. Seo, Y. Wang, J. Ma, Z. Ma, *IEEE Electron Device Lett.* **2013**, *34*, 160.
[19] G. Qin, T. Cai, H.-C. Yuan, J.-H. Seo, J. Ma, Z. Ma, *Appl. Phys. Lett.* **2014**, *104*, 163501.
[20] J. Yoon, A. J. Baca, S.-I. Park, P. Elvikis, J. B. Geddes, L. Li, R. H. Kim, J. Xiao, S. Wang, T.-H. Kim, M. J. Motala, B. Y. Ahn, E. B. Duoss, J. A. Lewis, R. G. Nuzzo, P. M. Ferreira, Y. Huang, A. Rockett, J. A. Rogers, *Nat. Mater.* **2008**, *7*, 907.

[21] W. Zhou, D. Zhao, Y.-C. Shuai, H. Yang, S. Chuwongin, A. Chadha, J.-H. Seo, K. X. Wang, V. Liu, Z. Ma, S. Fan, *Prog. Quantum Electron.* **2014**, *38*, 1.
[22] E. Lee, D.-I. Moon, J.-H. Yang, K. S. Lim, Y.-K. Choi, *IEEE Electron Device Lett.* **2009**, *30*, 493.
[23] Z. Huang, J. E. Carey, M. Liu, X. Guo, E. Mazur, J. C. Campbell, *Appl. Phys. Lett.* **2006**, *89*, 033506.
[24] M. C. Hamilton, S. Martin, J. Kanicki, *IEEE Trans. Electron Devices* **2004**, *51*, 877.
[25] P. Krogstrup, H. I. Jørgensen, M. Heiss, O. Demichel, J. V. Holm, M. Aagesen, J. Nygard, A. F. I. Morral, *Nat. Photonics* **2013**, *7*, 306.
[26] M. A. Green, M. Keevers, *Prog. Photovoltaics* **1995**, *3*, 189.
[27] S. M. Sze, K. K. Ng, *Physics of Semiconductor Devices*, 3rd ed., Wiley, New York **2006**.
[28] J. N. Kuo, H. W. Wu, G. B. Lee, Opt. Express 2006, 14, 6844.
[29] Y. Vygranenko, A. Nathan, M. Vieira, A. Sazonov, *Appl. Phys. Lett.* **2010**, *96*, 173507.
[30] H. C. Ko, M. P. Stoykovich, J. Song, V. Malyarchuk, W. M. Choi, C.-J. Yu, J. GeddesIII, J. Xiao, S. Wang, Y. Y. Huang, J. A. Rogers, *Nature* **2008**, *454*, 748.
[31] Y. M. Song, Y. Xie, V. Malyarchuk, J. Xiao, I. Jung, K.-J. Choi, Z. Liu, H. Park, C. Lu, R.-H. Kim, R. Li, K. B. Crozier, Y. Huang, J. A. Rogers, *Nature* **2013**, *497*, 95.